AIMS Mathematics, 8(12): 31050–31069.
DOI: 10.3934/math.20231589
Received: 17 September 2023
Revised: 26 October 2023
Accepted: 30 October 2023
Published: 20 November 2023

http://www.aimspress.com/journal/Math

Research article

Fractional-time derivative in ISPH method to simulate bioconvection flow of a rotated star in a hexagonal porous cavity

Abdelraheem M. Aly* and Abd-Allah Hyder

Department of Mathematics, College of Science, King Khalid University, P. O. Box 9004, Abha 61413, Saudi Arabia

* **Correspondence:** Email: ababdallah@kku.edu.sa; Tel: +966551323276.

Abstract: A novel treatment of fractional-time derivative using the incompressible smoothed particle hydrodynamics (ISPH) method is introduced to simulate the bioconvection flow of nano-enhanced phase change materials (NEPCM) in a porous hexagonal cavity. The fractional-time derivative is based on the Caputo style, which reflects the fractional order behavior in complex systems. In this work, the circular rotation of the embedded four-pointed star and the motion of oxytactic microorganisms in a hexagonal cavity are conducted. Due to the significance of fractional derivatives in handling real physical problems with more flexibility than conventional derivatives, the present scheme of the ISPH method is developed to solve the fractional-time derivative of the bioconvection flow in a porous hexagonal cavity. This study implicates the variations of a fractional-time derivative, a parametric of an inner four-pointed star, and the pertinent physical parameters on the behavior of a bioconvection flow of a nanofluid in a hexagonal-cavity containing oxytactic microorganisms. The presence of microorganisms has a significant role in many biological, engineering, and medical phenomena. From the present numerical investigation, it is well mentioned that the computational time of the transient processes can be reduced by applying a fractional-time derivative. The variable sizes of an inner four-pointed star enhance the bioconvection flow in a hexagonal cavity.

Keywords: fractional-time derivative; oxytactic microorganisms; four-pointed star; bioconvection flow; NEPCM
Mathematics Subject Classification: 26A33, 49M41, 76M27

1. Introduction

In recent years, scientists and researchers have been interested in expanding neuroscience by developing new types of nanotechnology. There has been an increasing amount of interest in nanofluids due to their enhancement of heat transfer [1,2]. Eastman et al. [3] reported that the development of nanofluids can enhance thermal conductivity by 40%. The size of nanoparticles is scaled (10-100 nm) and most nanoparticles are constructed of a few hundred atoms. Nanofluids can be applied to several industrial issues such as the cooling of electronic equipment, chemical processes, and heat exchangers [4–10].

Bioconvection flow naturally occurs when microorganism swim in an upwards motion within water. Commonly, the swimming microorganisms are denser than the water and their motion follows the changes of density and hydrodynamic inconstancy [11,12]. There are several uses of bioconvection flows in biotechnology, environmental sciences, and thermal engineering. There are two different models to examine the bioconvection flow of microorganisms' motion, namely the oxytactic and erratic motions. The theoretical investigations of the bioconvection flow of several kinds of motile microorganisms were developed by Hillesdon and Pedley [13] and Pedley et al. [14]. Yamamoto [15] introduced a numerical simulation using phototactic microalgae for bioconvection flow in a transparent circular channel. Shermet and Pop [16] examined the bioconvection flow of oxytactic microorganisms inside a porous cavity. Balla et al. [17] investigated the influence of thermal radiation on the bioconvection of oxytactic microorganisms inside a porous enclosure.

The studies of microorganisms within a nanofluid flow have an important role in enhancing the thermal conductivity of many techniques such as microfluid devices, bio-medical, enzyme biosensors, and chip microdevices. Several studies on the bioconvection flow of nanofluids are performed in [18–22]. Rashad and Nabwey [23] studied the mixed bioconvection flow of a nanofluid over a circular cylinder. Hussain et al. [22] adopted Galerkin finite element method to explore the impacts of magnetic force on the bioconvection flow of hybrid nanofluids inside a porous cavity containing gyrotactic microorganisms. Pekmen and Oztop [24] investigated the influence of a periodic magnetic field on the natural convection of a nanofluid with oxytactic bacteria in a cavity containing a conducting solid zone.

Phase change materials (PCM) are used to enhance heat transfer and are considered to be latent heat storage. The numerical/experimental investigations on the preparation of PCM and applications of PCM in enhancement heat transfer are discussed in references [25–29]. Liu et al. [30] reviewed the uses of NEPCM in thermal energy. There are many studies on the convective heat/mass transfer of NEPCM inside a microtube [31], a hexagonal cavity [32], a porous cavity [33], a porous grooved cavity [34], and a mini-channel heatsink [35].

The smoothed particle hydrodynamics (SPH) method has been widely applied in several fluid flow and solid mechanics applications due to its mesh-free Lagrangian nature and its ability to handle large deformations. The SPH method was initially developed independently by Gingold and Monaghan [36] and Lucy [37]. The incompressible version, entitled the ISPH method, is based on the projection method [38] and applied in several fields [39–44]. The ISPH method is implemented to emulate the bioconvection flow of NEPCM inside a porous annulus between circular cylinders [45]. Further studies on the magnetic effects on the bioconvection flow of NEPCM inside an annulus based on the ISPH method have been introduced by Alhejaili and Aly [46]. Due to the applications of NEPCM within storage equipment, the present work investigates the bioconvection of NEPCM inside a hexagonal cavity containing a four-pointed star, minimization of energy consumption, and thermal management, as well as the uses of bioconvection in

biotechnology, pharmaceutical industry, sustainable fuel cell and microbial oil recovery. The definition and salient features associated with fractional Caputo operations are mentioned below.

Due to its numerous applications across numerous domains, fractional evaluation equations have recently received a lot of attention [47,48]. There are numerous concepts of fractional derivatives and integrals in the literature. The most well-known of these fractional operators are Riemann-Liouville, Riesz, Caputo, and Grunwald-Letnikov [49,50]. These fractional ideas, which differ from conventional Newton-Leibniz calculus and are crucial in several application fields, are known for having the traits of non-locality and heredity [51]. The well-known product, quotient, and chain principles of derivative processes seem to no longer apply to these derivatives [52]. This deficiency results in various difficulties while tackling mathematical issues.

This work aims to develop the ISPH method via a time-fractional Caputo derivative in handling the bioconvection flow of NEPCM in a porous hexagonal cavity including a rotated four-pointed star. The main findings showed that a fractional-time derivative helps speed up the transition processes and can handle the physical problem with more flexibility. Hence, it is recommended to apply fractional-time derivatives for adjusting the time intervals at several applications in computational fluid dynamics. Due to the high porous resistance of a nanofluid flow at a lower Darcy number, the nanofluid's velocity decreases by 22.64% according to a reduction in Darcy number from 10^{-2} to 10^{-5}. Due to Lorentz's magnetic forces, an increase in Hartmann's number from 0 to 60 causes a decline in nanofluid velocity by 17.81%. The Rayleigh and bioconvection-Rayleigh numbers are considered the main factors in enhancing the strength of bioconvection flow and velocity field.

2. Model of the problem

Figure 1 indicates the primary diagram of the studied physical problem. The inner shape of a four-pointed star carries low-temperature T_c, oxygen concentration C_{min}, and microorganisms m_{min}. The vertical sides of the walls carry high temperatures T_h, oxygen concentration C_o, and oxytactic microorganisms m_o. The plane walls maintained at high temperatures T_h and adiabatic oxygen concentration C_o. The circular rotation of an inner four-pointed star is $\boldsymbol{V_c} = \omega(\boldsymbol{r} - \boldsymbol{r_o})$, where ω represents a frequency. These distributions are introduced separately in Figure 2. In this figure, an initial setting of hydrodynamic conditions such as material type, velocity field V, oxytactic microorganism N, temperature θ, and oxygen concentration φ for the studied physical problem are introduced. The physical properties of a porous medium, NEPCM (core and shell), and water as a base fluid are informed in Table 1. The description of the inner star shape as follows:

$$\frac{(x-x_0)^2}{a} + \frac{(y-y_0)^2}{b} \le r_c \quad \& \quad \frac{(x-x_0)^2}{b} + \frac{(y-y_0)^2}{a} \le r_c. \tag{1}$$

Table 1. The thermal properties of a suspension ([53]).

	k	ρ	$\beta \times 10^{-5}$	C_p
Porous medium	1.05	2700	------	840
Water	0.613	997.1	21	4179
Shell	------	721	------	2037
Core	------	786	17.28	1317.7

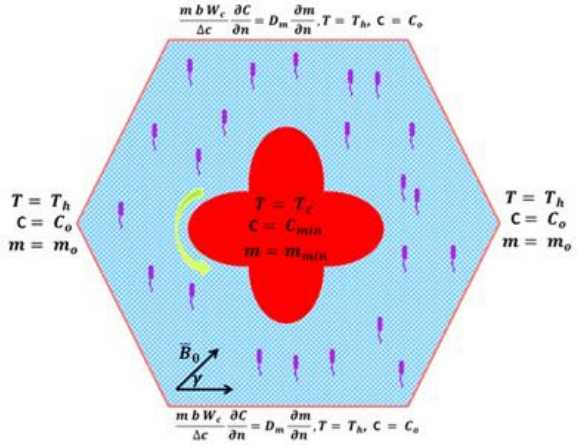

Figure 1. The primary diagram of the studied physical problem.

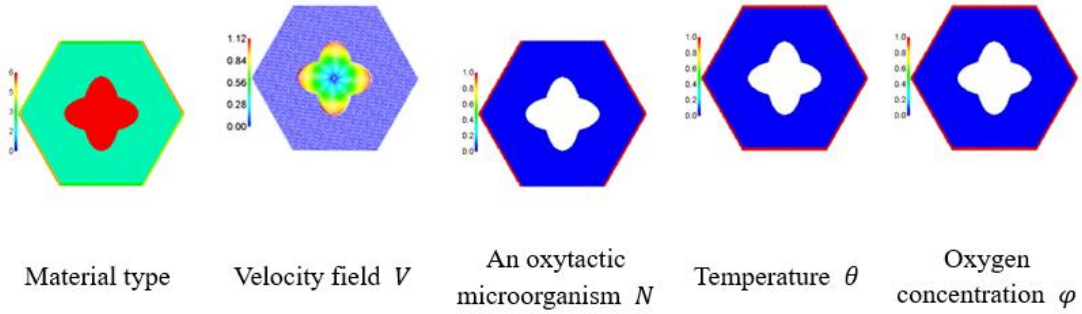

Figure 2. An initial setting of hydrodynamic conditions for the present model.

3. Mathematical analysis

In the literature, there are different formulations for fractional derivatives. The most often used fractional derivative is the Caputo derivative.

Definition 1. [54] For $\alpha \in \mathbb{C}$ with $Re(\alpha) > 0$, the fractional α-order Riemann-Liouville integral beginning with $\alpha > 0$ is defined as follows [54]:

$$\mathcal{J}_a^{\alpha} x(\tau) = \frac{1}{\Gamma(\alpha)} \int_a^{\tau} (m-a)^{\alpha-1}\, x(m) dm. \tag{2}$$

The fractional α-order Caputo derivative beginning with $a > 0$ is defined as follows:

$${}_a^C D_{\tau}^{\alpha} x(\tau) = \mathcal{J}_a^{n-\alpha} x^{(n)}(\tau) = \frac{1}{\Gamma(n-\alpha)} \int_a^{\tau} (m-a)^{\alpha-1}\, x^{(n)}(m) dm, \tag{3}$$

where $[\alpha] = n - 1$. For simplicity, we write D_{τ}^{α} instead of ${}_a^C D_{\tau}^{\alpha}$.

Theorem 2. If Z is endlessly α −differentiable on a region around a point v, then the expansion of Z's power fractional power series is as follows:

$$Z(\tau)=\sum_{a=0}^{A}\frac{(D_{\tau}^{\alpha}Z)(v)(\tau-z)^{a\alpha}}{\alpha^{a}a!},\qquad v<\tau<\Upsilon^{1/\alpha},\ \Upsilon>0. \tag{4}$$

To devote the ISPH structure for resolving time-fractional models, we frame in the following symbolizations. Let $F\in\mathbb{N}$, $c<C\in\mathbb{R}_{+}$ and $\tau_n=n\,\Delta\tau+c$, $n=0,\dots,F$ be an identical dividing up of the interval $[c,C]$. Here, $\Delta\tau=\tau_n-\tau_{n-1}$ is the constant step size and $Z(\tau_n)$ can be denoted by Z_n.

Theorem 3. If Z is endlessly $\alpha-$differentiable on a region around a point $\mathrm{v}_1\in(\mathrm{v},\infty)$, then, Z has the following fractional series expansion:

$$Z(\tau)=Z(v)+\frac{(D_{\tau}^{\alpha}u)(v)\Psi_1}{\alpha}+\frac{(D_{\tau}^{\alpha}u)^{(2)}(v_1)\Psi_2}{2\alpha^2}+\frac{(D_{\tau}^{\alpha}u)^{(3)}(v_1)\Psi_3}{3!\,\alpha^3}+\frac{(D_{\tau}^{\alpha}Z)^{(4)}(v_1)\Psi_4}{4!\,\alpha^4}+\Upsilon(\tau,v_1,v), \tag{5}$$

where $\Upsilon(\tau,v_1,v)$ represents the reminder, $\Psi_1=\Sigma_1^{\alpha}-\Sigma_2^{\alpha}$, $\Psi_2=\Sigma_1^{2\alpha}-\Sigma_2^{2\alpha}-2\Sigma_2^{\alpha}\Psi_1$, $\Psi_3=\Sigma_1^{3\alpha}-\Sigma_2^{3\alpha}-3\Sigma_2^{\alpha}\Psi_2-3\Sigma_2^{2\alpha}\Psi_1$, $\Psi_4=\Sigma_1^{4\alpha}-\Sigma_2^{4\alpha}-4\Sigma_2^{\alpha}\Psi_3-6\Sigma_2^{2\alpha}\Psi_2-4\Sigma_2^{3\alpha}\Psi_1$, $\Sigma_1=\tau-v$, and $\Sigma_2=v_1-v$.

Assume $Z(\tau)$ solves a fractional system with $0<\alpha\leq 1$. Due to Theorem 3, the fractional Taylor expansion of $Z(\tau_{n+1})$ at $\tau=\tau$ implies the following [55]:

$$Z(\tau_{n+1})=Z(\tau_n)+\frac{(\Delta\tau)^{\alpha}((n+1)^{\alpha}-n^{\alpha})}{\alpha}(D_{\tau}^{\alpha}Z)(\tau_n)+\Upsilon(\tau_{n+1},\tau_n,v). \tag{6}$$

The ISPH method is a particle-based, mesh-free and Lagrangian computational method. The fractional-time derivatives of dimensionless controlling equations are as follows:

$$\frac{\partial U}{\partial X}+\frac{\partial V}{\partial Y}=0, \tag{7}$$

$$\frac{1}{\varepsilon}D_{\tau}^{\alpha}U=-\frac{\rho_f}{\rho_b}\frac{\partial P}{\partial X}+\frac{\mu_b}{\varepsilon\mu_f}\frac{\rho_f}{\rho_b}Pr\left(\frac{\partial^2\mathrm{U}}{\partial X^2}+\frac{\partial^2\mathrm{U}}{\partial Y^2}\right)-\frac{\mu_b}{\mu_f}\frac{\rho_f}{\rho_b}Pr\frac{U}{Da}-\frac{1.75}{\sqrt{150}}\frac{1}{\sqrt{Da\varepsilon^3}}U\sqrt{U^2+V^2}+\frac{\sigma_b}{\sigma_f}\frac{\rho_f}{\rho_b}PrHa^2(V\,sin\gamma\,cos\gamma-Usin^2\gamma), \tag{8}$$

$$\frac{1}{\varepsilon}D_{\tau}^{\alpha}V=-\frac{\rho_f}{\rho_b}\frac{\partial P}{\partial Y}+\frac{\mu_b}{\varepsilon\mu_f}\frac{\rho_f}{\rho_b}Pr\left(\frac{\partial^2\mathrm{V}}{\partial X^2}+\frac{\partial^2\mathrm{V}}{\partial Y^2}\right)+\frac{(\rho\beta)_b}{(\rho\beta)_f}\frac{\rho_f}{\rho_b}Ra\,Pr(\theta-Ra_b)-\frac{\mu_b}{\mu_f}\frac{\rho_f}{\rho_b}Pr\frac{V}{Da}-\frac{1.75}{\sqrt{150}}\frac{1}{\sqrt{Da\varepsilon^3}}V\sqrt{U^2+V^2}+\frac{\sigma_b}{\sigma_f}\frac{\rho_f}{\rho_b}PrHa^2(U\,sin\gamma\,cos\gamma-Vcos^2\gamma), \tag{9}$$

$$\left(\varepsilon Cr+(1-\varepsilon)\frac{(\rho C)_s}{(\rho C)_f}\right)D_{\tau}^{\alpha}\theta=\frac{k_{m,b}}{k_f}\left(\frac{\partial^2\theta}{\partial X^2}+\frac{\partial^2\theta}{\partial Y^2}\right), \tag{10}$$

$$D_\tau^\alpha \varphi = \frac{1}{Le}\left(\frac{\partial^2 \varphi}{\partial X^2} + \frac{\partial^2 \varphi}{\partial Y^2}\right) - \frac{\sigma}{Le} N, \tag{11}$$

$$\chi D_\tau^\alpha N = \frac{1}{Le}\left(\frac{\partial^2 N}{\partial X^2} + \frac{\partial^2 N}{\partial Y^2}\right) - \frac{Pe}{Le}\left(N\left(\frac{\partial^2 \varphi}{\partial X^2} + \frac{\partial^2 \varphi}{\partial Y^2}\right) + \frac{\partial N}{\partial X}\frac{\partial \varphi}{\partial X} + \frac{\partial N}{\partial Y}\frac{\partial \varphi}{\partial Y}\right). \tag{12}$$

The dimensionless set is as follows:

$$\begin{gathered} X = \frac{x}{L}, \quad Y = \frac{y}{L}, \quad U = \frac{uL}{\zeta_f}, V = \frac{vL}{\zeta_f}, \quad \theta = \frac{T - T_c}{T_h - T_c}, N = \frac{m}{m_0}, \quad P = \frac{pL^2}{\rho_f \zeta_f^2}, \\ \tau = \frac{t\zeta_f}{L^2}, \quad \chi = \frac{D_c}{D_m}, \phi = \frac{C - C_{min}}{C_o - C_{min}}, \end{gathered} \tag{13}$$

The dimensionless boundary conditions are as follows:

$$\begin{gathered} \text{Outer walls: } \theta = 0, \varphi = 0, U = 0, V = 0, Pe\mathrm{N}\frac{\partial \varphi}{\partial n} - \frac{\partial N}{\partial n} = 0, \\ \text{Inner fins: } \theta = 0,\ U = 0, V = 0\ \varphi = 1, N = 1, \\ \text{Inner wavy cylinder: } \theta = 1,\ U = U_{rot}, V = V_{rot},\ \mathrm{N} = 1, \varphi = 1. \end{gathered} \tag{14}$$

The average $\overline{Nu}$ and $\overline{Sh}$ are as follows:

$$\overline{Nu} = \frac{-1}{L_h}\int_0^{L_h} \frac{k_{m,b}}{k_f}\frac{\partial \theta}{\partial \boldsymbol{n}}\, d\zeta, \tag{15}$$

$$\overline{Sh} = \frac{-1}{L_h}\int_0^{L_h} \frac{\partial \varphi}{\partial \boldsymbol{n}}\, d\zeta. \tag{16}$$

4. Results and discussion

This section represents the obtained numerical simulations of the time-fractional derivative of the bioconvection flow of NEPCM in a porous hexagonal cavity containing oxytactic microorganisms and a rotated four-pointed star shape. The time-fractional factor α is varied from 0.9 to 1, the dimensionless time τ reached 0.16, the length parameters of an inner four-pointed star a varied from 0.2 to 0.7 and b varied from 0.05 to 0.1. The bioconvection Rayleigh number Ra_b is varied from 0 to 1000, Darcy's number Da is varied from 10^{-2} to 10^{-5}, the Hartmann number Ha is varied from 0 to 60, and the Lewis number Le is varied from 1 to 20. The Rayleigh number Ra is varied from 10^3 to 10^6 and the solid volume fraction ϕ is varied from 0 to 0.08. Due to the importance of fractional-time derivatives in the treatment of real physical problems, the effects of the time-

fractional derivative α on the contours of Cr, N, θ, and velocity field $\boldsymbol{V}$ as well as the average $\overline{Nu}$ and $\overline{Sh}$ at different time instants $\tau = 0.01, 0.02, 0.05$, and 0.16 are presented in Figures 3–7. Here, when $\alpha = 1$ gives a conventional-time derivative without considering the fractional case when $\alpha < 1$ gives a fractional-time derivative. Thus, at $\tau \leq 0.02$, the contours of Cr are dramatically influenced by the variation of α. The physical meaning is that low values for α speed up the transition processes from an unsteady to a steady state. The new fractional-time derivative based on the Caputo style is more effective in speeding up the transition process compared to the recent studies in [45,46]. Generally, the rotation of an inner four-pointed star is affected by the variation of α due to the dependence of rotational motion on the fractional-time derivative of their locations. At $\tau \geq 0.05$, the contours of Cr are almost similar under the variations of α, which confirms the previous note on speeding up the transition processes by the fractional-time derivative α. Then, it is well mentioned the fractional-space derivative of governing equations is significantly and rapidly needed. Figure 4 represents the effects of α on the contours of N at time instants $\tau = 0.01, 0.02, 0.05$ and 0.16. Here, the contours of N are dramatically influenced by an increment in α. The distributions of N soon reached a steady state regardless of the rotation of an inner four-pointed star when $\alpha = 0.9$. As a result, the computational time of the transient processes can be reduced by applying a fractional-time derivative. In addition, due to speeding up the transition processes, it is recommended to apply fractional-time derivatives for adjusting the time intervals at delayed simulations compared to the experimental data. Figure 5 depicts the effects of the fractional-time derivative factor α on the isotherms θ at different time instants $\tau = 0.01, 0.02, 0.05$, and 0.16. At $\tau \leq 0.02$, the lower value of α supports the transient processes which shows that the isotherms are completely over the star shape inside the hexagonal cavity. The strength of the isotherms shrinks across the hexagonal cavity when α increases. Whilst, at $\tau \geq 0.05$, the isotherms have reached the steady state and there are almost no changes on the isotherms under a change on α. Figure 6 represents the effects of the fractional-time derivative factor α on the velocity field V at time instants $\tau = 0.01, 0.02, 0.05$ and 0.16. The velocity field is influenced by the variations of α due to the changes in the circular rotation of an inner four-pointed star. At the steady state $\tau \geq 0.16$, the velocity's maximum increases as α increases. The observed contributions of α in changing the strength of the velocity field, as well as the distributions of isotherms, oxytactic microorganisms, and the heat capacity ratio, are significant. Hence, it is well-mentioned that the need for fractional calculus in computational fluid dynamics still requires more attention. Figure 7 depicts the effects of the fractional-time derivative factor α on the average $\overline{Nu}$ and $\overline{Sh}$. As α increases from 0.9 to 1, the average $\overline{Nu}$ decreases by 9.63% and the average $\overline{Sh}$ decreases by 13.32%.

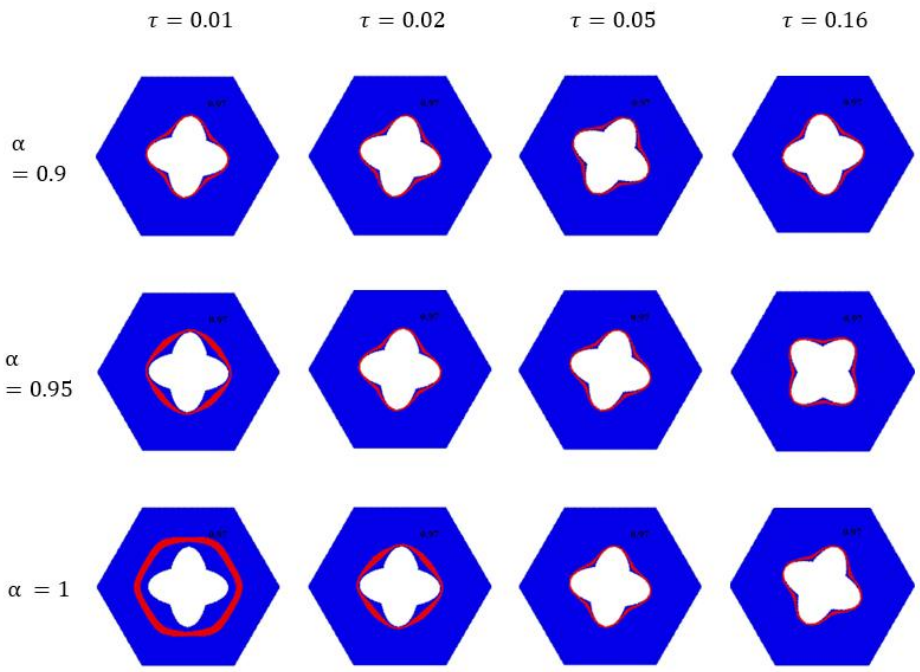

Figure 3. Effects of fractional-time derivative factor α on the contours of Cr at time instants $\tau = 0.01, 0.02, 0.05$ and 0.16 when $Da = 10^{-3}$, $N = 2$, $\sigma = 1$, $Pe = 1$, $Le = 10$, $\theta_f = 0.05$, $Ra = 10^4$, $Ra_b = 10$, $\phi = 0.05$, $Ha = 20$, $a = 0.1$ and $b = 0.4$.

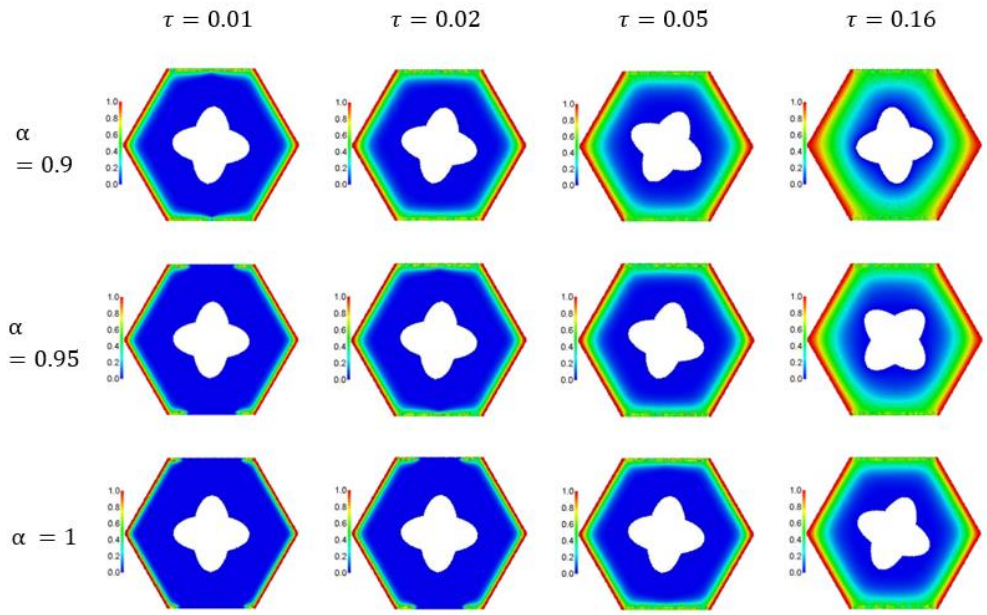

Figure 4. Effects of fractional-time derivative factor α on the contours of N at time instants $\tau = 0.01, 0.02, 0.05$ and 0.16 when $Da = 10^{-3}$, $N = 2, \sigma = 1$, $Pe = 1$, $Le = 10$, $\theta_f = 0.05$, $Ra = 10^4$, $\phi = 0.05$, $Ra_b = 10$, $Ha = 20$, $a = 0.1$ and $b = 0.4$.

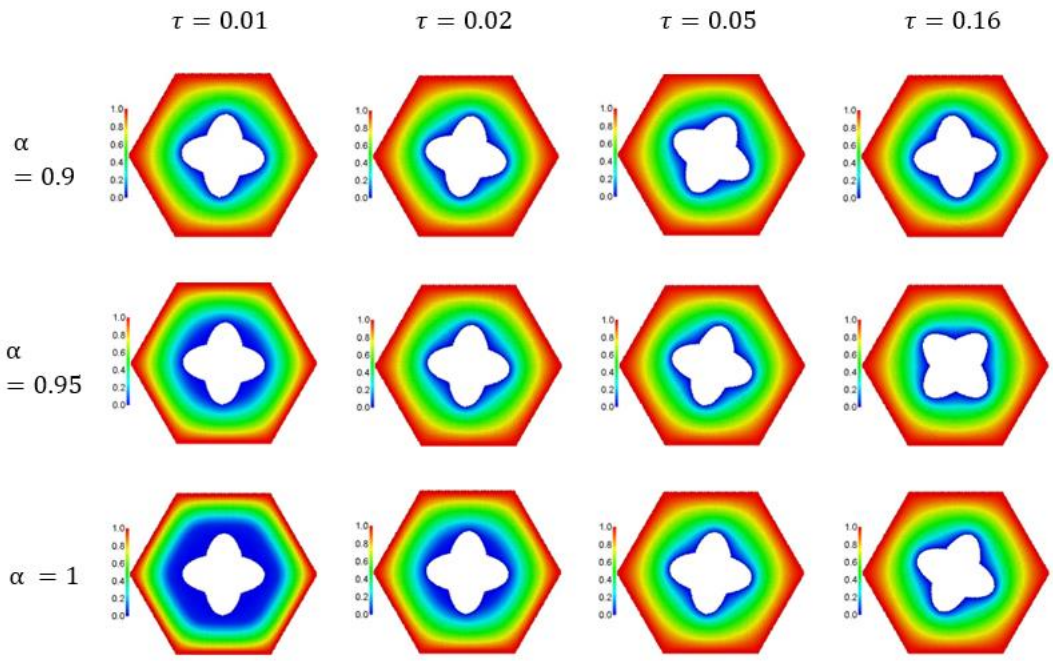

Figure 5. Effects of fractional-time derivative factor α on the isotherms θ at time instants $\tau = 0.01, 0.02, 0.05$ and 0.16 when $Da = 10^{-3}$, $N = 2$, $\sigma = 1$, $Pe = 1$, $Le = 10$, $\theta_f = 0.05$, $Ra = 10^4$, $\phi = 0.05$, $Ra_b = 10$, $Ha = 20$, $a = 0.1$ and $b = 0.4$.

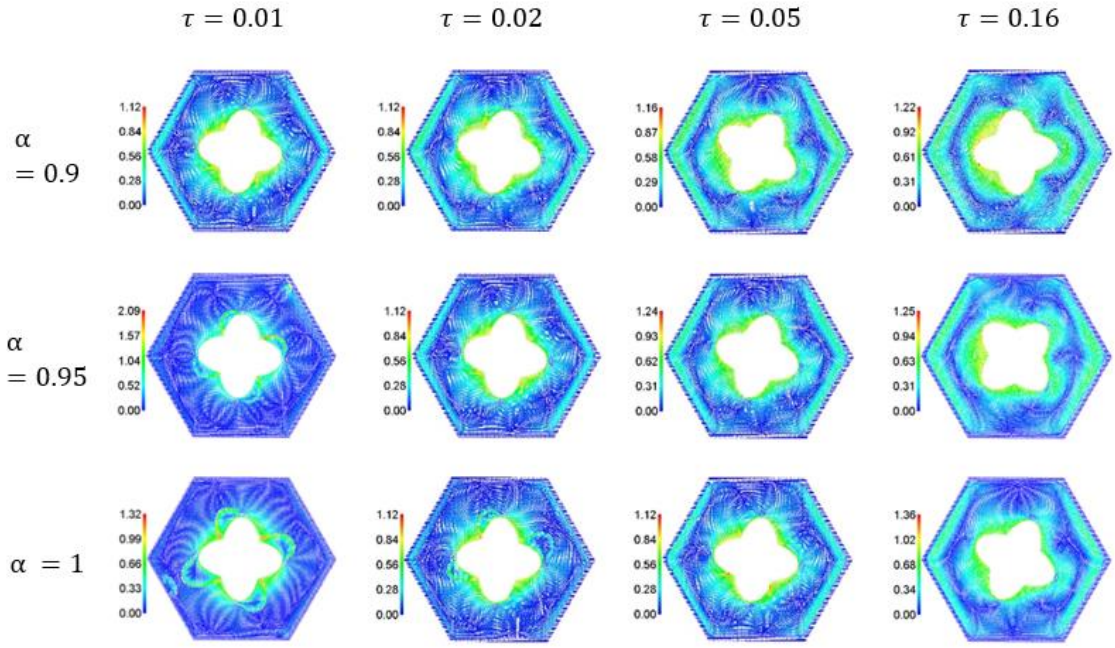

Figure 6. Effects of fractional-time derivative factor α on the velocity field $\boldsymbol{V}$ at time instants $\tau = 0.01, 0.02, 0.05$ and 0.16 when $Da = 10^{-3}$, $N = 2$, $\sigma = 1$, $Pe = 1, Le = 10$, $\theta_f = 0.05$, $Ra = 10^4$, $\phi = 0.05$, $Ra_b = 10, Ha = 20$, $a = 0.1$ and $b = 0.4$.

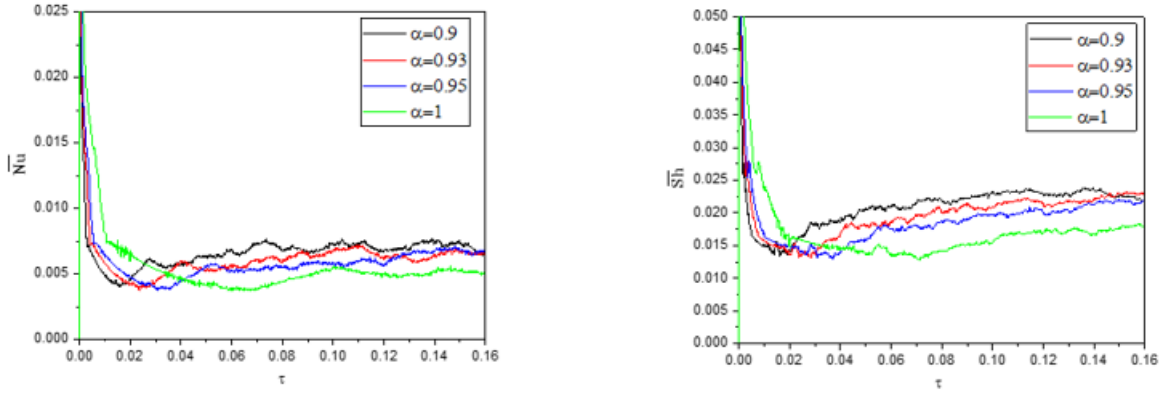

Figure 7. Effects of fractional-time derivative factor α on the average $\overline{Nu}$ and $\overline{Sh}$ at $\tau = 0.16$, $Da = 10^{-3}$, $N = 2$, $\sigma = 1$, $Pe = 1$, $Ha = 20$, $Le = 10$, $\theta_f = 0.05$, $Ra = 10^4$, $\phi = 0.05$, $a = 0.1$, $Ra_b = 10$ and $b = 0.4$.

Figures 8 and 9 represent the effects of length parameters of an inner four-pointed star a & b on the contours of Cr, N, $\boldsymbol{V}$ and θ, as well as the average $\overline{Nu}$ and $\overline{Sh}$. In Figure 8, the contours of Cr are formed around the cool shape of a four-pointed star at any size of an inner star shape. The contours of N and isotherms are affected by variations of the inner star sizes. Also, the velocity field is influenced by the variations in an inner star's size. In Figure 9, the average $\overline{Nu}$ is enhanced according to an increment in the size of an inner star and the average $\overline{Sh}$ is slightly changed under the changes in an inner star's size. Hence, the size of an inner star is effective in controlling the distributions of the hydrodynamics properties and nanofluid flow. The contribution of sizes for an embedded star in enhancing heat/mass transfer within a hexagonal cavity is more clarified in this article compared to previous studies in [45,46]. Figure 10 indicates the effects of the bioconvection Rayleigh number Ra_b on the contours of Cr, N, $\boldsymbol{V}$ and θ. As the Ra_b represents a main factor in bioconvection flow, an increase in Ra_b dramatically enhances the strength of oxytactic microorganisms and velocity field in a hexagonal cavity. There are slight variations in the isotherms and contours of Cr under the changes of Ra_b. In this work, due to the numerous bioconvection flows in the pharmaceutical industry, microbial-boosted oil recovery, ecological fuel cell equipment and biotechnology, the contributions of Ra_b in enhancing bioconvection flow, as well as the nanofluid's velocity, represent their important roles. Figure 11 represents the effects of Darcy number Da on the contours of Cr, N, $\boldsymbol{V}$ and θ. Physically, the Darcy number Da signifies the ratio influence between the medium's permeability to the cross-sectional area of a medium. Consequently, a reduction in Da slightly reduces the contours of Cr, oxytactic microorganisms, and isotherms. The velocity field shrinks by 22.64% as Da decreases from 10^{-2} to 10^{-5}. Figure 12 shows the effects of the Hartmann number Ha on the contours of Cr, N, $\boldsymbol{V}$ and θ. The Hartmann number Ha represents the relationship between electromagnetic and viscous forces. Increasing Ha supports the Lorentz forces that shrink the nanofluid's velocity. Accordingly, the nanofluid's velocity decreases by 17.81% as Ha boosts from 0 to 60. There are minor changes in the contours of Cr, N, and θ under the variations of Ha. Figure 13 indicates the effects of the Lewis number Le on $\boldsymbol{V}$ and contours of φ. As Le increases from 1 to 20, the velocity field shrinks by 28.31%. A Lewis number is defined as the relative of thermal to mass diffusivity. Due to the consumption of oxygen at a higher mass

diffusivity, the oxygen concentration strongly decreases as Le boosts. Figure 14 introduces the effects of the Rayleigh number Ra on the contours of Cr, N, $\boldsymbol{V}$ and θ. The Rayleigh number Ra represents a buoyancy-driven flow and describes the fluid's flow regime. Therefore, an increase in Ra augments the strength of the isotherms, as well as the contours of N, φ, Cr and θ. There is a strong enhancement in the velocity field according to an augmentation in Ra. A Physical reason returns to higher buoyancy forces that augments the nanofluid's velocity. Figure 15 presents the effects of the solid volume fraction ϕ on the contours of Cr, N, $\boldsymbol{V}$ and θ. The solid volume fraction ϕ signifies the volume of solid particles divided by the total volume of a suspension. Here, to avoid solidification between the porous media and a nanofluid, the addition of solid nanoparticles is limited to 8%. It is noted that the addition of solid nanoparticles up to 8% shrinks the nanofluid velocity due to the extra viscosity of a nanofluid. There are minor reductions in the isotherms, oxygen concentration and oxytactic microorganisms under the augmentations in ϕ.

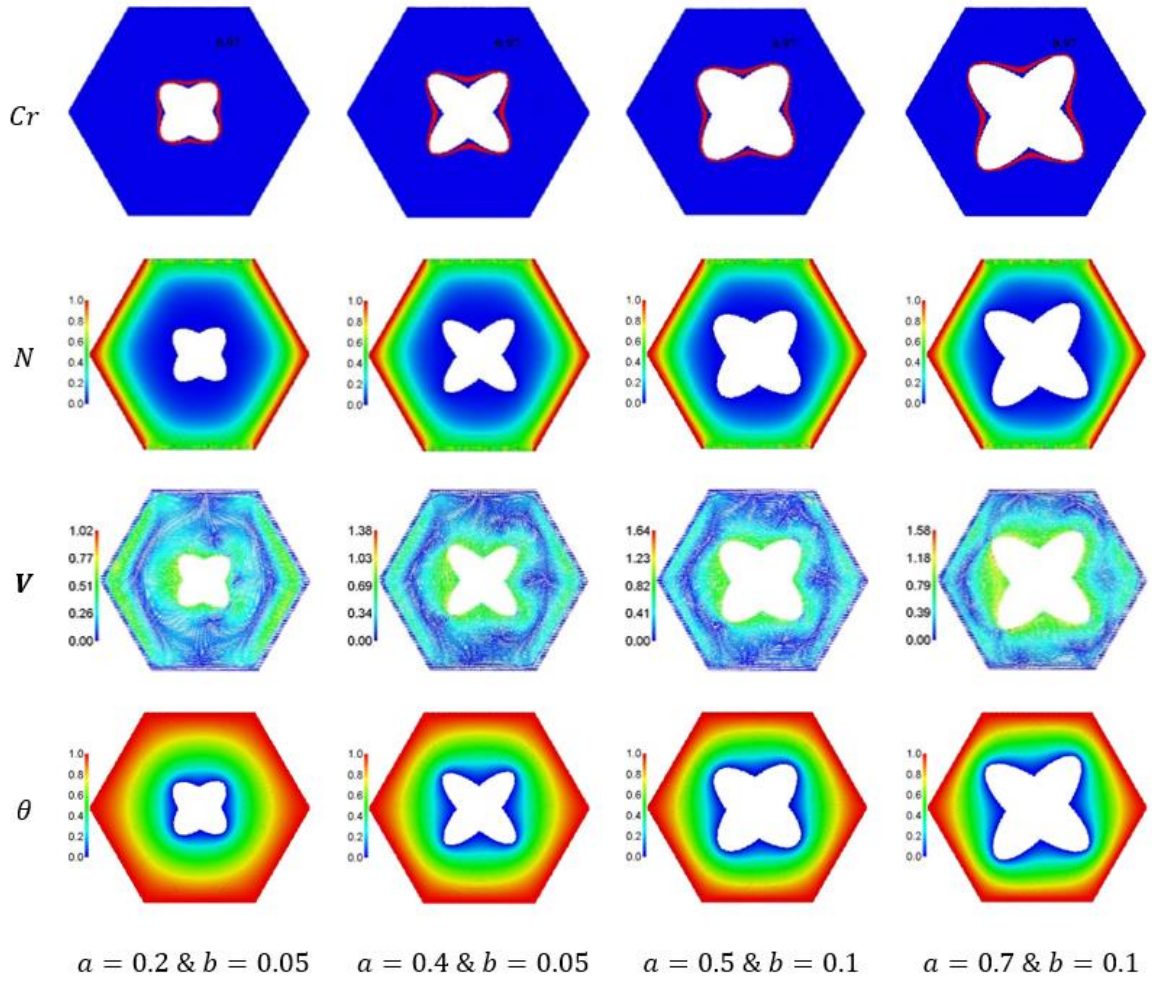

Figure 8. Effects of length parameters of an inner four-pointed star a & b on the contours of Cr, N, $\boldsymbol{V}$ and θ at $\alpha = 0.96$, $\tau = 0.16$, $Da = 10^{-3}$, $Ha = 20$, $N = 2$, $\sigma = 1$, $Pe = 1$, $Le = 10$, $\theta_f = 0.05$, $Ra = 10^4$, $Ra_b = 10$ and $\phi = 0.05$.

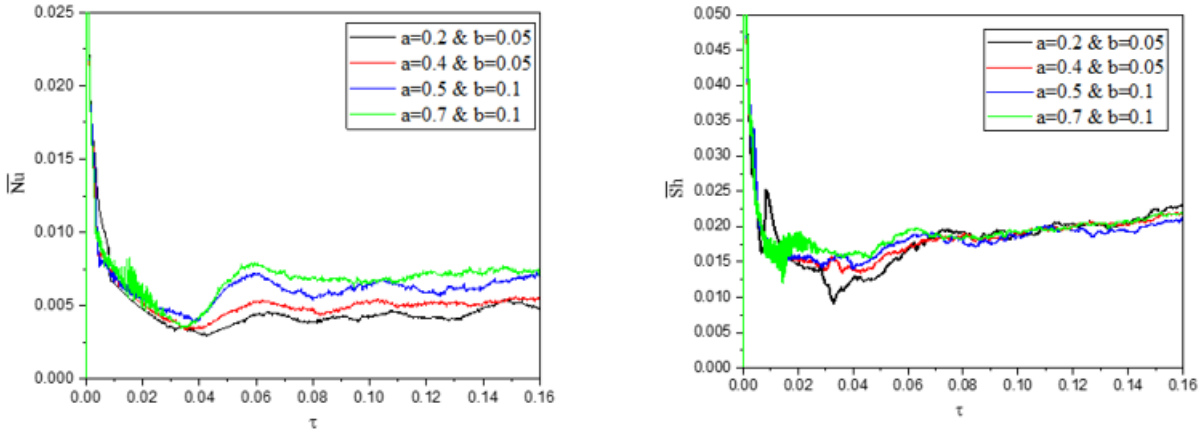

Figure 9. Effects of length parameters of an inner four-pointed star a & b on the average $\overline{Nu}$ and $\overline{Sh}$ at $\alpha = 0.96$, $\tau = 0.16$, $Da = 10^{-3}$, $N = 2$, $\sigma = 1$, $Pe = 1$, $Ha = 20$, $Le = 10$, $\theta_f = 0.05$, $Ra = 10^4$, $Ra_b = 10$ and $\phi = 0.05$.

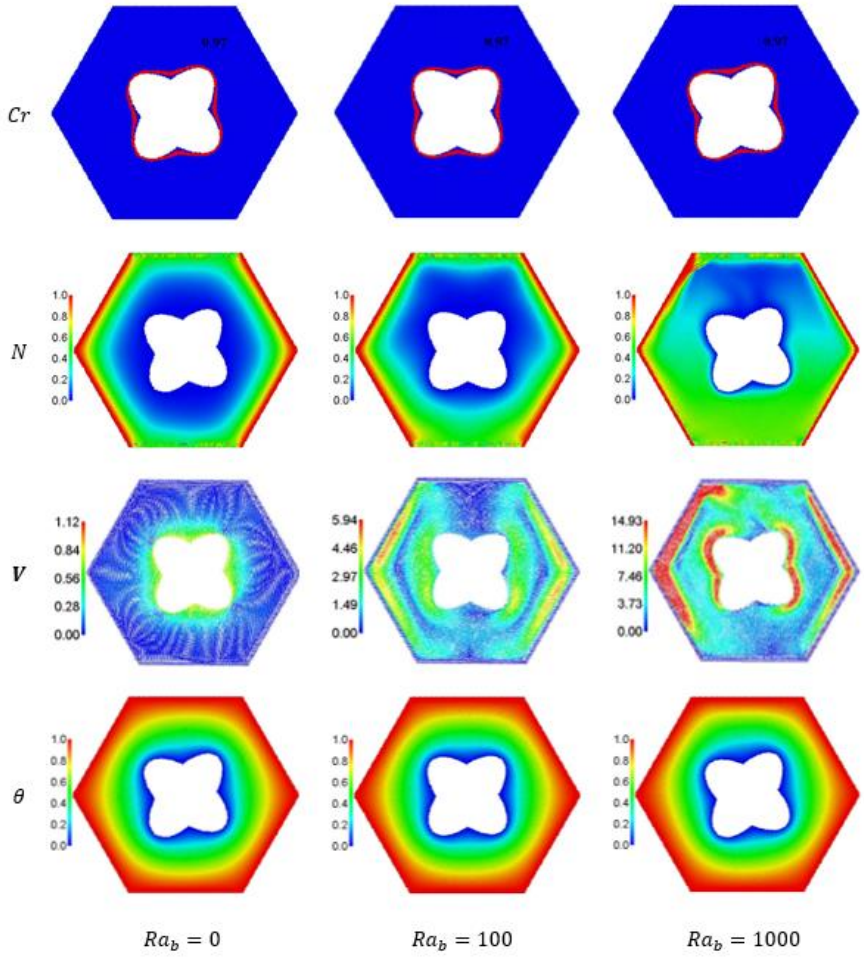

Figure 10. Effects of bioconvection Rayleigh number Ra_b on the contours of Cr, N, $\boldsymbol{V}$ and θ at $\alpha = 0.96$, $\tau = 0.16$, $Da = 10^{-3}$, $Ha = 20$, $N = 2$, $\sigma = 1$, $Pe = 1$, $Le = 10$, $\theta_f = 0.05$, $Ra = 10^4$, $\phi = 0.05$, $a = 0.1$ and $b = 0.4$.

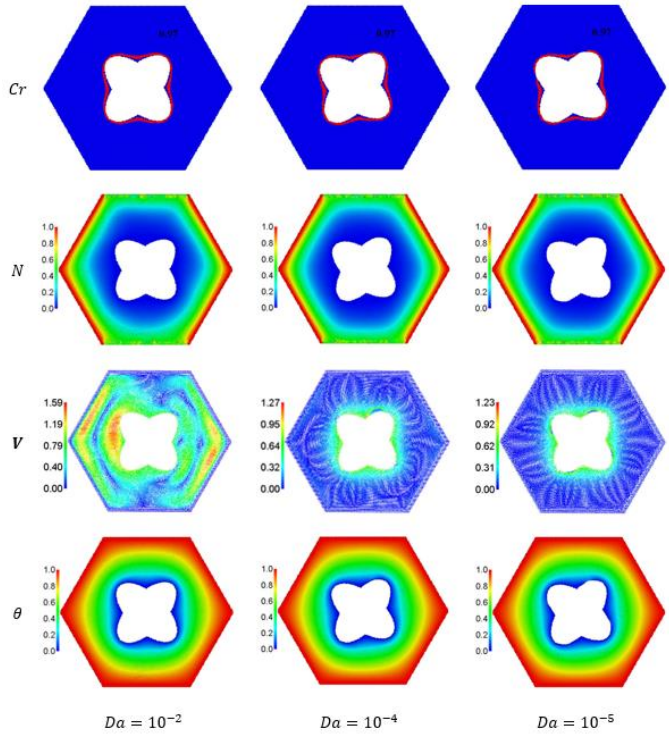

Figure 11. Effects of Darcy number Da on the contours of Cr, N, $\boldsymbol{V}$ and θ at $Ra_b = 10, \alpha = 0.96,\ \tau = 0.16,\ Ha = 20,\ N = 2,\ \sigma = 1,\ Pe = 1,\ Le = 10,\ \theta_f = 0.05,\ Ra = 10^4,\ \phi = 0.05, a = 0.1$ and $b = 0.4$.

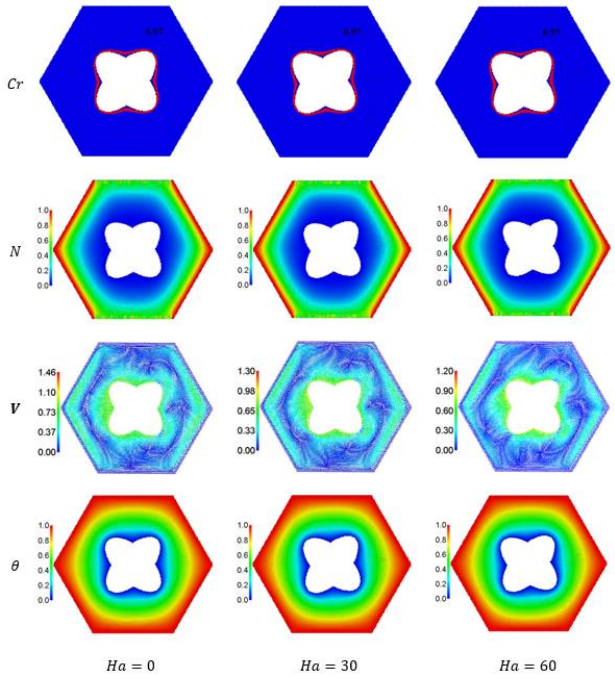

Figure 12. Effects of Hartmann number Ha on the contours of Cr, N, $\boldsymbol{V}$ and θ at $Ra_b = 10,\ \alpha = 0.96,\ \tau = 0.16,\ Da = 10^{-3},\ N = 2,\ \sigma = 1,\ Pe = 1,\ Le = 10,\ \theta_f = 0.05,\ Ra = 10^4,\ \phi = 0.05,\ a = 0.1$ and $b = 0.4$.

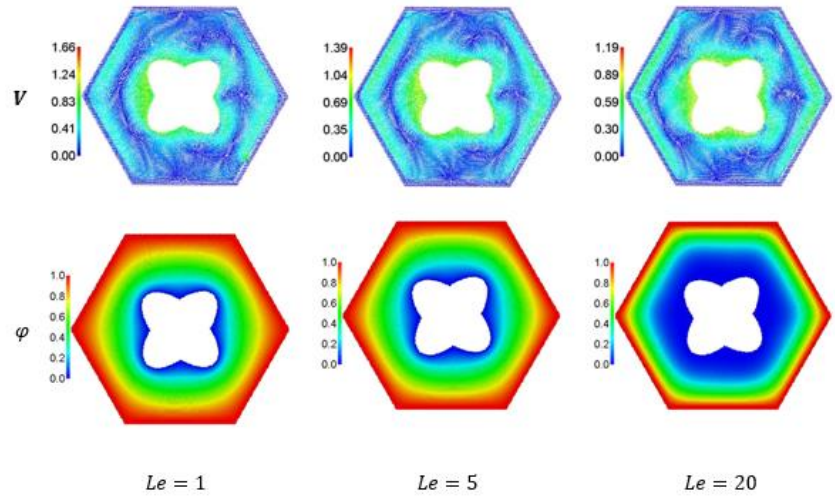

Figure 13. Effects of Lewis number Le on $\boldsymbol{V}$ and contours of φ at $Ra_b = 10$, $\alpha = 0.96$, $\tau = 0.16$, $Da = 10^{-3}$, $N = 2, \sigma = 1$, $Pe = 1$, $Ha = 20$, $\theta_f = 0.05$, $Ra = 10^4$, $\phi = 0.05$, $a = 0.1$ and $b = 0.4$.

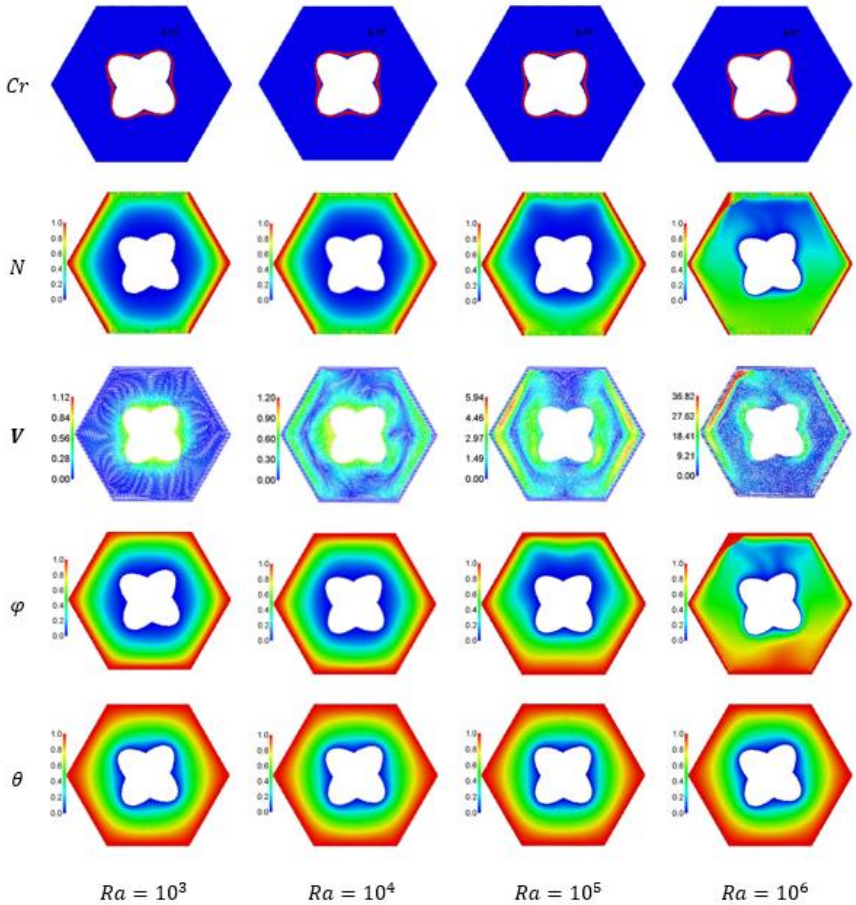

Figure 14. Effects of Rayleigh number Ra on the contours of Cr, N, $\boldsymbol{V}$ and θ at $Ha = 20, Ra_b = 10$, $\alpha = 0.96$, $\tau = 0.16$, $Da = 10^{-3}$, $N = 2$, $\sigma = 1$, $Pe = 1$, $Le = 10$, $\theta_f = 0.05$, $\phi = 0.05$, $a = 0.1$ and $b = 0.4$.

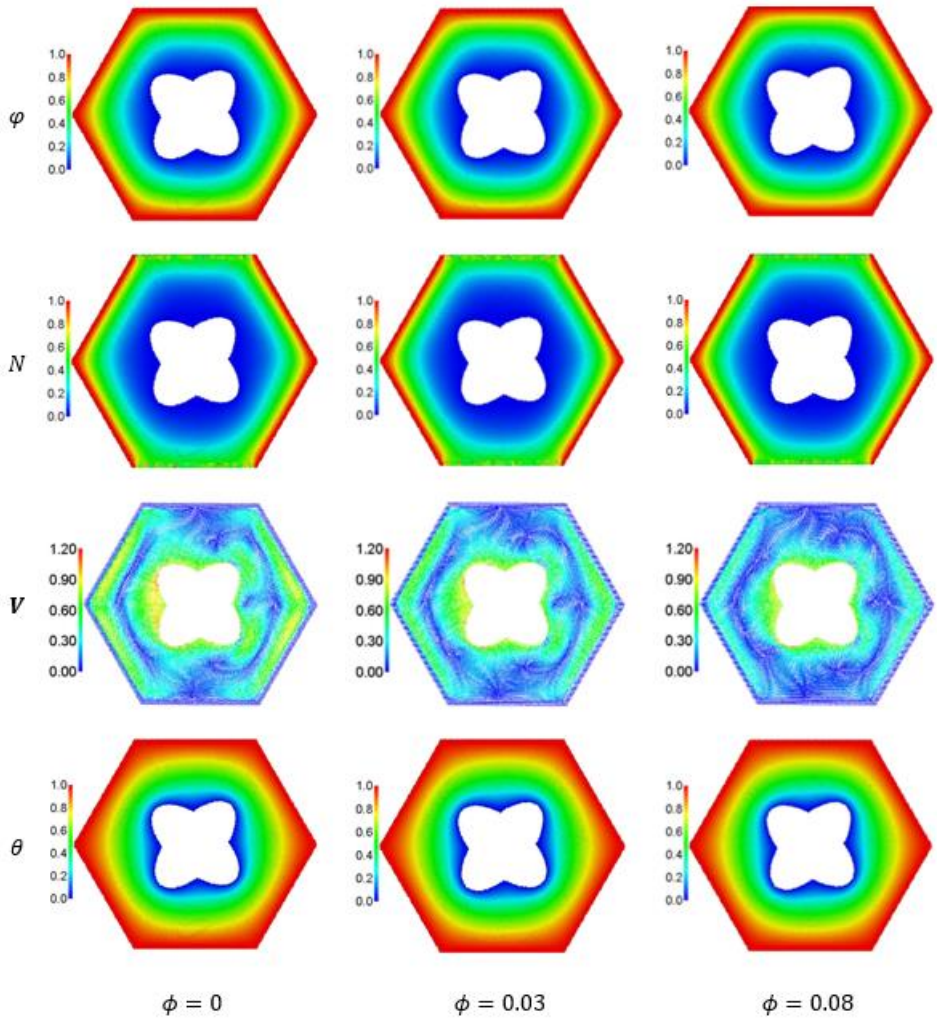

Figure 15. Effects of solid volume fraction ϕ on the contours of Cr, N, $\boldsymbol{V}$ and θ at $Ha = 20$, $Ra_b = 10$, $\alpha = 0.96$, $\tau = 0.16$, $Da = 10^{-3}$, $N = 2$, $\sigma = 1$, $Pe = 1$, $Le = 10, \theta_f = 0.05$, $a = 0.1$ and $b = 0.4$

5. Conclusions

The present work has a novelty in developing the fractional-time derivative on the ISPH method to simulate the bioconvection flow of NEPCM in a porous hexagonal cavity. The circular rotation of an embedded four-pointed star is considered. The major findings of this study are as follows:

1) The fractional-time derivative of the ISPH method speeds up the transient processes and it can handle the physical problem with more flexibility. It is recommended to apply the fractional-time derivative in computational fluid dynamics since it has flexibility in handling the physical problem and can reduce the computational time.

2) The size of an inner four-pointed star is effective in enhancing the bioconvection flow and nanofluid velocity that can be applied in electronic devices and thermal industries.

3) The Rayleigh and bioconvection Rayleigh numbers work well to enhance the bioconvection flow and nanofluid's velocity in a hexagonal cavity.

4) Due to high porous resistance at lower values of Darcy number, the nanofluid's velocity declines

by a reduction in Darcy number. Additionally, the nanofluid's velocity reduces according to an increment in Hartmann number and the addition of nanoparticles.

5) As a future study, it is recommended to extend the fractional calculus in space for the governing equations and expand the fractional calculus in computational fluid dynamics.

As a future work, space-time fractional derivatives can be applied to the ISPH method in simulating convection flows in complex geometries. Furthermore, double parameter fractional derivatives will be employed in the ISPH method to obtain more realistic physical results of convection flows.

Use of AI tools declaration

The authors declare they have not used Artificial Intelligence (AI) tools in the creation of this article.

Acknowledgments

The authors extend their appreciation to the Deanship of Scientific Research at King Khalid University, Abha, Saudi Arabia, for funding this work through the Research Group Project under Grant Number (RGP. 2/102/44).

Conflict of interest

The authors declare that they have no known competing financial interests or personal relationships that could have appeared to influence the work reported in this paper.

References

1. S. U. S. Choi, J. A. Eastman, Enhancing thermal conductivity of fluids with nanoparticles, *ASME International Mechanical Engineering Congress & Exposition*, San Francisco, 1995.
2. S. K. Das, S. U. Choi, W. Yu, T. Pradeep, *Nanofluids: science and technology*, New York: John Wiley & Sons, 2007.
3. J. A. Eastman, U. S. Choi, S. Li, L. J. Thompson, S. Lee, Enhanced thermal conductivity through the development of nanofluids, *MRS Online Proceedings Library*, **457** (1996), 3–11. https://doi.org/10.1557/PROC-457-3
4. J. Buongiorno, L. W. Hu, Innovative technologies: two-phase heat transfer in water-based nanofluids for nuclear applications final report, *Nuclear Engineering Education Research (NEER) Program*, 2009. https://doi.org/10.2172/958216
5. N. Putra, Yanuar, F. N. Iskandar, Application of nanofluids to a heat pipe liquid-block and the thermoelectric cooling of electronic equipment, *Exp. Therm. Fluid Sci.*, **35** (2011), 1274–1281. https://doi.org/10.1016/j.expthermflusci.2011.04.015
6. O. Mahian, A. Kianifar, S. A. Kalogirou, I. Pop, S. Wongwises, A review of the applications of nanofluids in solar energy, *Int. J. Heat Mass Tran.*, **57** (2013), 582–594. https://doi.org/10.1016/j.ijheatmasstransfer.2012.10.037

7. S. Rashidi, O. Mahian, E. M. Languri, Applications of nanofluids in condensing and evaporating systems, *J. Therm. Anal. Calorim.*, **131** (2018), 2027–2039. https://doi.org/10.1007/s10973-017-6773-7
8. M. A. Nazari, M. H. Ahmadi, M. Sadeghzadeh, M. B. Shafii, M. Goodarzi, A review on application of nanofluid in various types of heat pipes, *J. Cent. South Univ.*, **26** (2019), 1021–1041. https://doi.org/10.1007/s11771-019-4068-9
9. J. Li, X. Zhang, B. Xu, M. Yuan, Nanofluid research and applications: a review, *Int. J. Heat Mass Tran.*, **127** (2021), 105543. https://doi.org/10.1016/j.icheatmasstransfer
10. M. A. Sheremet, Applications of Nanofluids, *Nanomaterials (Basel)*, **11** (2021), 1716. https://doi.org/10.3390/nano11071716
11. A. V. Kuznetsov, The onset of thermo-bioconvection in a shallow fluid saturated porous layer heated from below in a suspension of oxytactic microorganisms, *Eur. J. Mech. B-Fluid.*, **25** (2006), 223–233. https://doi.org/10.1016/j.euromechflu.2005.06.003
12. A. V. Kuznetsov, Nanofluid bioconvection in water-based suspensions containing nanoparticles and oxytactic microorganisms: oscillatory instability, *Nanoscale Res. Lett.*, **6** (2011), 100. https://doi.org/10.1186/1556-276X-6-100
13. A. J. Hillesdon, T. J. Pedley, Bioconvection in suspensions of oxytactic bacteria: linear theory, *J. Fluid Mech.*, **324** (1996), 223–259. https://doi.org/10.1017/S0022112096007902
14. T. J. Pedley, N. A. Hill, J. O. Kessler, The growth of bioconvection patterns in a uniform suspension of gyrotactic micro-organisms, *J. Fluid Mech.*, **195** (1988), 223–237. https://doi.org/10.1017/S0022112088002393
15. T. Yamamoto, Numerical simulation of the flows of phototactic microalgae suspensions in an illuminated circular channel, *Nihon Reoroji Gakk.*, **43** (2015) 53–62. https://doi.org/10.1678/rheology.43.53
16. M. A. Sheremet, I. Pop, Thermo-bioconvection in a square porous cavity filled by oxytactic microorganisms, *Transp. Porous Med.*, **103** (2014), 191–205. https://doi.org/10.1007/s11242-014-0297-4
17. C. S. Balla, A. Ramesh, N. Kishan, A. M. Rashad, Z. M. A. Abdelrahman, Bioconvection in oxytactic microorganism-saturated porous square enclosure with thermal radiation impact, *J. Therm. Anal. Calorim.*, **140** (2020), 2387–2395. https://doi.org/10.1007/s10973-019-09009-7
18. S. Ahmad, M. Ashraf, K. Ali, Bioconvection due to gyrotactic microbes in a nanofluid flow through a porous medium, *Heliyon*, **6** (2020), e05832. https://doi.org/10.1016/j.heliyon.2020.e05832
19. D. K. Mandal, N. Biswas, N. K. Manna, R. S. R. Gorla, A. J. Chamkha, Role of surface undulation during mixed bioconvective nanofluid flow in porous media in presence of oxytactic bacteria and magnetic fields, *Int. J. Mech. Sci.*, **211** (2021), 106778. https://doi.org/10.1016/j.ijmecsci.2021.106778
20. N. Biswas, D. K. Mandal, N. K. Manna, A. C. Benim, Magneto-hydrothermal triple-convection in a W-shaped porous cavity containing oxytactic bacteria, *Sci. Rep.*, **12** (2022), 18053. https://doi.org/10.1038/s41598-022-18401-7
21. M. Habibishandiz, Z. Saghir, MHD mixed convection heat transfer of nanofluid containing oxytactic microorganisms inside a vertical annular porous cylinder, *International Journal of Thermofluids*, **14** (2022), 100151. https://doi.org/10.1016/j.ijft.2022.100151

22. S. Hussain, A. M. Aly, H. F. Öztop, Magneto-bioconvection flow of hybrid nanofluid in the presence of oxytactic bacteria in a lid-driven cavity with a streamlined obstacle, *Int. Commun. Heat Mass*, **134** (2022), 106029. https://doi.org/10.1016/j.icheatmasstransfer.2022.106029
23. A. M. Rashad, H. A. Nabwey, Gyrotactic mixed bioconvection flow of a nanofluid past a circular cylinder with convective boundary condition, *J. Taiwan Inst. Chem. E.*, **99** (2019), 9–17. https://doi.org/10.1016/j.jtice.2019.02.035
24. B. P. Geridonmez, H. F. Oztop, Conjugate natural convection flow of a nanofluid with oxytactic bacteria under the effect of a periodic magnetic field, *J. Magn. Magn. Mater.*, **564** (2022), 170135. https://doi.org/10.1016/j.jmmm.2022.170135
25. B. Chen, X. Wang, R. Zeng, Y. Zhang, X. Wang, J. Niu, et al., An experimental study of convective heat transfer with microencapsulated phase change material suspension: Laminar flow in a circular tube under constant heat flux, *Exp. Therm. Fluid Sci.*, **32** (2008), 1638–1646. https://doi.org/10.1016/j.expthermflusci.2008.05.008
26. W. Wu, H. Bostanci, L. C. Chow, Y. Hong, C. M. Wang, M. Su, et al., Heat transfer enhancement of PAO in microchannel heat exchanger using nano-encapsulated phase change indium particles, *Int. J. Heat Mass Tran.*, **58** (2013), 348–355. https://doi.org/10.1016/j.ijheatmasstransfer.2012.11.032
27. C. J. Smith, P. M. Forster, R. Crook, Global analysis of photovoltaic energy output enhanced by phase change material cooling, *Appl. Energ.*, **126** (2014), 21–28. https://doi.org/10.1016/j.apenergy.2014.03.083
28. W. Su, J. Darkwa, G. Kokogiannakis, Review of solid-liquid phase change materials and their encapsulation technologies, *Renew. Sust. Energ. Rev.*, **48** (2015), 373–391. https://doi.org/10.1016/j.rser.2015.04.044
29. Y. Pahamli, M. J. Hosseini, A. A. Ranjbar, R. Bahrampoury, Analysis of the effect of eccentricity and operational parameters in PCM-filled single-pass shell and tube heat exchangers, *Renew. Energ.*, **97** (2016), 344–357. https://doi.org/10.1016/j.renene.2016.05.090
30. C. Liu, Z. Rao, J. Zhao, Y. Huo, Y. Li, Review on nanoencapsulated phase change materials: Preparation, characterization and heat transfer enhancement, *Nano Energy*, **13** (2015), 814–826. https://doi.org/10.1016/j.nanoen.2015.02.016
31. H. R. Seyf, Z. Zhou, H. B. Ma, Y. Zhang, Three dimensional numerical study of heat-transfer enhancement by nano-encapsulated phase change material slurry in microtube heat sinks with tangential impingement, *Int. J. Heat Mass Tran.*, **56** (2013), 561–573. https://doi.org/10.1016/j.ijheatmasstransfer.2012.08.052
32. M. Ghalambaz, S. A. M. Mehryan, I. Zahmatkesh, A. Chamkha, Free convection heat transfer analysis of a suspension of nano-encapsulated phase change materials (NEPCMs) in an inclined porous cavity, *Int. J. Therm. Sci.*, **157** (2020), 106503. https://doi.org/10.1016/j.ijthermalsci.2020.106503
33. S. A. M. Mehryan, M. Ismael, M. Ghalambaz, Local thermal nonequilibrium conjugate natural convection of nano-encapsulated phase change particles in a partially porous enclosure, *Math. Method. Appl. Sci.*, **2020** (2020), 6338. https://doi.org/10.1002/mma.6338
34. S. Hussain, N. Alsedias, A. M. Aly, Natural convection of a water-based suspension containing nano-encapsulated phase change material in a porous grooved cavity, *J. Energy Storage*, **51** (2022), 104589. https://doi.org/10.1016/j.est.2022.104589

35. C. J. Ho, Y. C. Liu, T. F. Yang, M. Ghalambaz, W. M. Yan, Convective heat transfer of nano-encapsulated phase change material suspension in a divergent minichannel heatsink, *Int. J. Heat Mass Tran.*, **165** (2021), 120717. https://doi.org/10.1016/j.ijheatmasstransfer.2020.120717
36. R. A. Gingold, J. J. Monaghan, Smoothed particle hydrodynamics: theory and application to non-spherical stars, *Mon. Not. R. Astron. Soc.*, **181** (1977), 375–389. https://doi.org/10.1093/mnras/181.3.375
37. L. B. Lucy, A numerical approach to the testing of the fission hypothesis, *Astron. J.*, **82** (1977), 1013–1024. https://doi.org/10.1086/112164
38. S. J. Cummins, M. Rudman, An SPH projection method, *J. Comput. Phys.*, **152** (1999), 584–607. https://doi.org/10.1006/jcph.1999.6246
39. M. Asai, A. M. Aly, Y. Sonoda, Y. Sakai, A stabilized incompressible SPH method by relaxing the density invariance condition, *J. Appl. Math.*, **2012** (2012), 139583. https://doi.org/10.1155/2012/139583
40. F. Garoosi, A. Shakibaeinia, Numerical simulation of entropy generation due to natural convection heat transfer using Kernel Derivative-Free (KDF) Incompressible Smoothed Particle Hydrodynamics (ISPH) model, *Int. J. Heat Mass Tran.*, **150** (2020), 119377. https://doi.org/10.1016/j.ijheatmasstransfer.2020.119377
41. A. M. Aly, Mixing between solid and fluid particles during natural convection flow of a nanofluid-filled H-shaped cavity with three center gates using ISPH method, *Int. J. Heat Mass Tran.*, **157** (2020), 119803. https://doi.org/10.1016/j.ijheatmasstransfer.2020.119803
42. A. M. Aly, A. M. Yousef, N. Alsedais, MHD double diffusion of a nanofluid within a porous annulus using a time fractional derivative of the ISPH method, *Int. J. Mod. Phys. C*, **33** (2021), 2250056. https://doi.org/10.1142/S0129183122500565
43. Y. Shimizu, H. Gotoh, A. Khayyer, K. Kita, Fundamental investigation on the applicability of higher-order consistent ISPH method, *Int. J. Offshore Polar*, **32** (22022), 275–284. https://doi.org/10.17736/ijope.2022.jc868
44. A. M. Salehizadeh, A. R. Shafiei, A coupled ISPH-TLSPH method for simulating fluid-elastic structure interaction problems, *J. Marine. Sci. Appl.*, **21** (2022), 15–36. https://doi.org/10.1007/s11804-022-00260-3
45. N. Alsedais, A. Al-Hanaya, A. M. Aly, Magneto-bioconvection flow in a porous annulus between circular cylinders containing oxytactic microorganisms and NEPCM, *Int. J. Numer. Method. H.*, **33** (2023), 3228–3254. https://doi.org/10.1108/HFF-02-2023-0095
46. W. Alhejaili, A. M. Aly, Magneto-bioconvection flow in an annulus between circular cylinders containing oxytactic microorganisms, *Int. Commun. Heat Mass*, **146** (2023), 106893. https://doi.org/10.1016/j.icheatmasstransfer.2023.106893
47. A. Alaria, A. M. Khan, D. L. Suthar, D. Kumar, Application of fractional operators in modelling for charge carrier transport in amorphous semiconductor with multiple trapping, *Int. J. Appl. Comput. Math.*, **5** (2019), 167. https://doi.org/10.1007/s40819-019-0750-8
48. M. M. A. Khater, D. Baleanu, On abundant new solutions of two fractional complex models, *Adv. Differ. Equ.*, **2020** (2020), 268. https://doi.org/10.1186/s13662-020-02705-x
49. A. Hyder, A. H. Soliman, A new generalized θ-conformable calculus and its applications in mathematical physics, *Phys. Scr.*, **96** (2020), 015208. https://doi.org/10.1088/1402-4896/abc6d9
50. A. Hyder, M. A. Barakat, Novel improved fractional operators and their scientific applications, *Adv. Differ. Equ.*, **2021** (2021), 389. https://doi.org/10.1186/s13662-021-03547-x

51. A. Hyder, M. A. Barakat, A. Fathallah, C. Cesarano, Further integral inequalities through some generalized fractional integral operators, *Fractal Fract.*, **5** (2021), 282. https://doi.org/10.3390/fractalfract5040282
52. T. Abdeljawad, On conformable fractional calculus, *J. Comput. Appl. Math.*, **279** (2015), 57–66. https://doi.org/10.1016/j.cam.2014.10.016
53. M. Ghalambaz, A. J. Chamkha, D. Wen, Natural convective flow and heat transfer of Nano-Encapsulated Phase Change Materials (NEPCMs) in a cavity, *Int. J. Heat Mass Tran.*, **138** (2019), 738–749. https://doi.org/10.1016/j.ijheatmasstransfer.2019.04.037
54. I. Podlubny, *Fractional differential equations: An introduction to fractional derivatives, fractional differential equations, to methods of their solution and some of their applications*, San Diego: Academic Press, 1999.
55. Ş. Toprakseven, Numerical solutions of conformable fractional differential equations by Taylor and finite difference methods, *Süleyman Demirel Üniversitesi Fen Bilimleri Enstitüsü Dergisi*, **23** (2019), 850–863. https://doi.org/ 10.19113/sdufenbed.579361

AIMS Press